Nanoscale Characterization of Space Weathered Lunar Samples

A. M. Grice, P. C. Stancil, M. Ghafari, S. Singh, S. Gamage, M. J. Schiable, Y. Abate, K. Lang , and T. M Orlando

1. Supplementary Experimental Approach

For all samples, flake exfoliation and mounting used an adhesive strip placed onto a small piece of polydimethylsiloxane (PMDS) with the adhesive side facing down. The PMDS was then placed onto a microscope slide and pressure was applied to the back of the adhesive strip. After 1-2 hours of applied pressure, the adhesive strip was removed, leaving the sample flake embedded into the PDMS. A microscope was used to ensure the desired flake had transferred properly. Once the sample flake was confirmed to have transferred onto the PDMS, the PDMS was then set into a platform where it could be raised and lowered with enhanced precision. The PDMS was then lowered onto a silicon substrate and slowly removed to ensure a proper transfer of the sample flake onto the silicon substrate. Once visual confirmation of the transfer was obtained through the use of a microscope, the sample flake was then taken through the rest of the experimental procedure.

For the Nano-FTIR measurements, the amplitude and phase IR near-field spectra were normalized by collecting reference spectrum from an area on the Si substrate used to hold the sample flakes and then taking spectra at the appropriate sample locations. The reference spectrum was then divided into the sample spectrum, in the case of amplitude data [S_n(sample)/S_n(reference)], or subtracted from the sample spectrum, in the case of phase data [ϕ_n(sample)-ϕ_n(reference)]. Likewise for the PL measurements, the reference spectra were subtracted from the sample spectra.

The lunar samples from which the scanned flakes were taken, 15445 and 12016, are well known to contain high levels of olivine, pyroxene, and plagioclase minerals. Online spectral databases were initially used to isolate potential matches for the experimental spectra obtained from the lunar samples. Afterwards, several potential matches were selected, and spectra of the selected matches were taken experimentally to corroborate the spectra obtained from the online database.

In total four terrestrial minerals were selected as potential contributors to the spectra seen within the lunar scans. Anorthite, an end member of the plagioclase series of minerals defined by its high percentage of $CaAl_2Si_2O_8$, has a distinct peak at 915 cm^{-1}. Albite, the other endmember of the plagioclase series, is defined by its high percentage of $NaAlSi_3O_8$ and shows peaks between 1050 and 1250 cm^{-1}.

Forsterite, often called white olivine, is a magnesium rich endmember of the olivine series and shows a large distinct peak at around 900 cm^{-1}. The final mineral, enstatite, is a Mg-rich endmember of the pyroxene silicate series and displays peaks between 850 and 1080 cm^{-1}. Nano-FTIR and photoluminesence spectra of the terrestrial analogs and the lunar samples are shown in Figure S1. Fits to the lunar PL spectra are illustrated in Figures S2-S6 and summarized in Figure 2a. The best matches of the Nano-FTIR lunar samples to the terrestrial samples are given in Figure 2b and 2c of the manuscript.

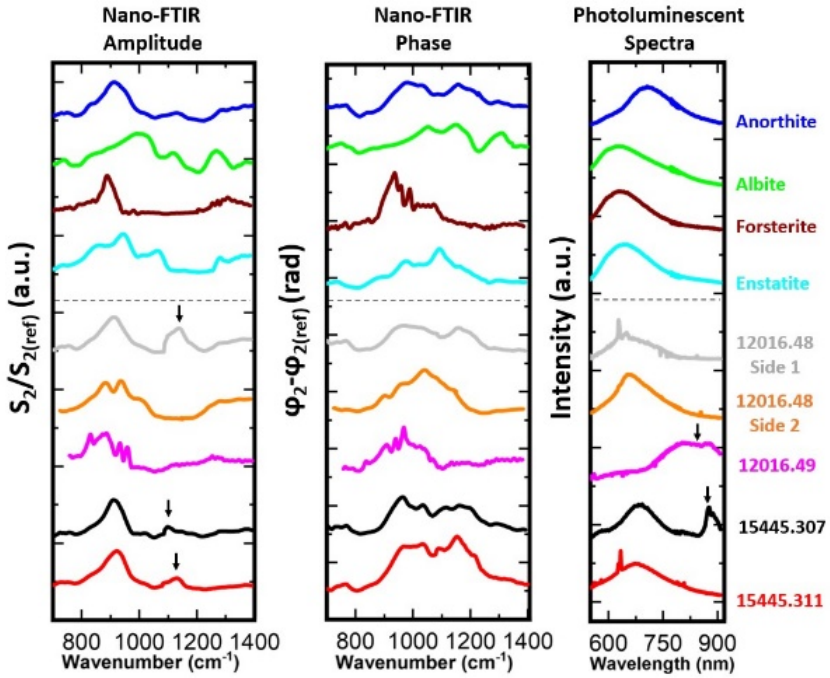

Figure S1. Representative amplitude, phase, and photoluminescent spectra from each terrestrial and lunar sample are presented in three columns for ease of comparison. Each set of spectra are color coded and labelled for the sample they represent. Peaks of interest that appear in lunar samples, but not their terrestrial analogs have been marked with arrows.

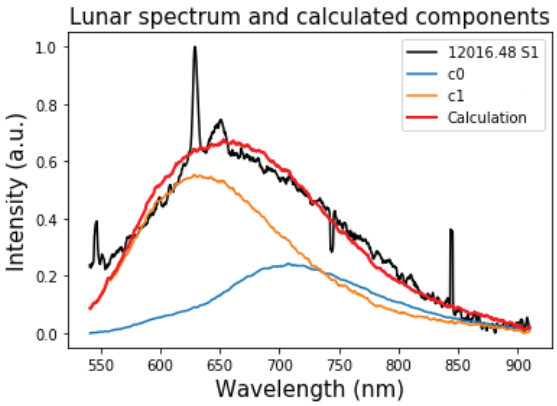

Figure S2. Photoluminescent spectrum of lunar sample 12016.48 S1 (black) along with appropriately scaled components used in the least squares fitting procedure and result of the fit calculation (red). Here c0 represents anorthite photoluminescent spectrum (blue) and c1 represents forsterite photoluminescent spectrum (orange).

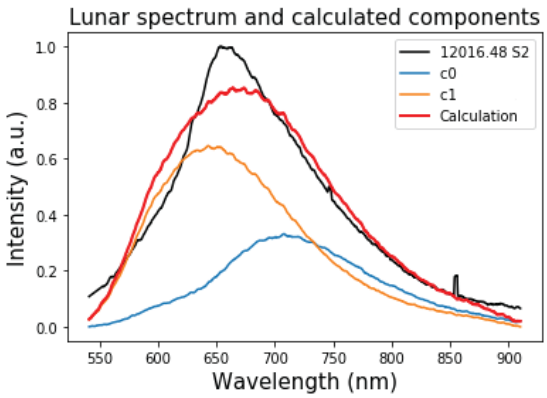

Figure S3. Photoluminescent spectrum of lunar sample 12016.48 S2 (black) along with appropriately scaled components used in the least squares fitting procedure and result of the fit calculation (red). Here c0 represents anorthite photoluminescent spectrum (blue) and c1 represents enstatite photoluminescent spectrum (orange).

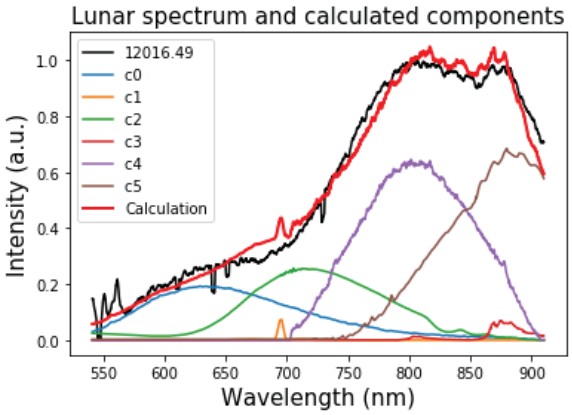

Figure S4. Photoluminescent spectrum of lunar sample 12016.49 (black) along with appropriately scaled components used in the least squares fitting procedure and result of the fit calculation (red). Here the following photoluminescent spectra are represented; c0 = forsterite (blue), c1 = Al_2O_3 (orange), c2 = MgO (green), c3 = Nd^{3+} (dark red), c4 = Cr^{3+} (purple), c5 = electron trap state (brown).

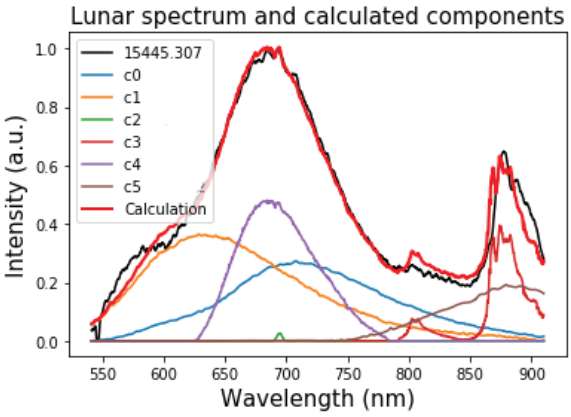

Figure S5. Photoluminescent spectrum of lunar sample 15445.307 (black) along with appropriately scaled components used in the least squares fitting procedure and result of the fit calculation (red). Here the following photoluminescent spectra are represented; c0 = anorthite (blue), c1 = forsterite (orange), c2 = Al_2O_3 (green), c3 = Nd^{3+} (dark red), c4 = Fe^{3+} (purple), c5 = electron trap state (brown).

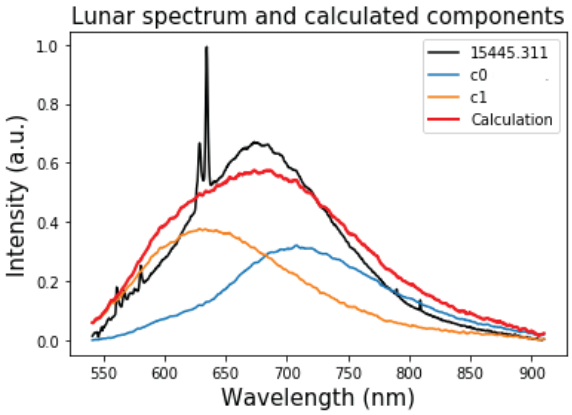

Figure S6. Photoluminescent spectrum of lunar sample 15445.311 (black) along with appropriately scaled components used in the least squares fitting procedure and result of the fit calculation (red). Here c0 represents anorthite photoluminescent spectrum (blue) and c1 represents forsterite photoluminescent spectrum (orange).

2. Shock-Induced Nano-FTIR Phase Enhancements

As described in the main text, single frequency Nano-FTIR maps were obtained at 935 and 1050 cm^{-1} on 2000 nm x 2000 nm regions of 15445.307 and 15445.311. Figure S7 shows the phase maps corresponding to Figure 4, while Figure S8 gives the topology for the region chosen for 15445.307. Figure S9 displays the phase difference for both samples corresponding to the amplitude ratio bins proposed by Martin et al. [1] (compared to the amplitude ratios in Figure 4e). While a systematic study of the phase differences for other samples is needed, it is of note that the phase difference for pressures greater than 25 GPa fall primarily between 1.3π and 1.6π implying a correlation with enhanced absorption at 1050 cm^{-1}, roughly independent of the 935 cm^{-1} phase, with impact-induced shock.

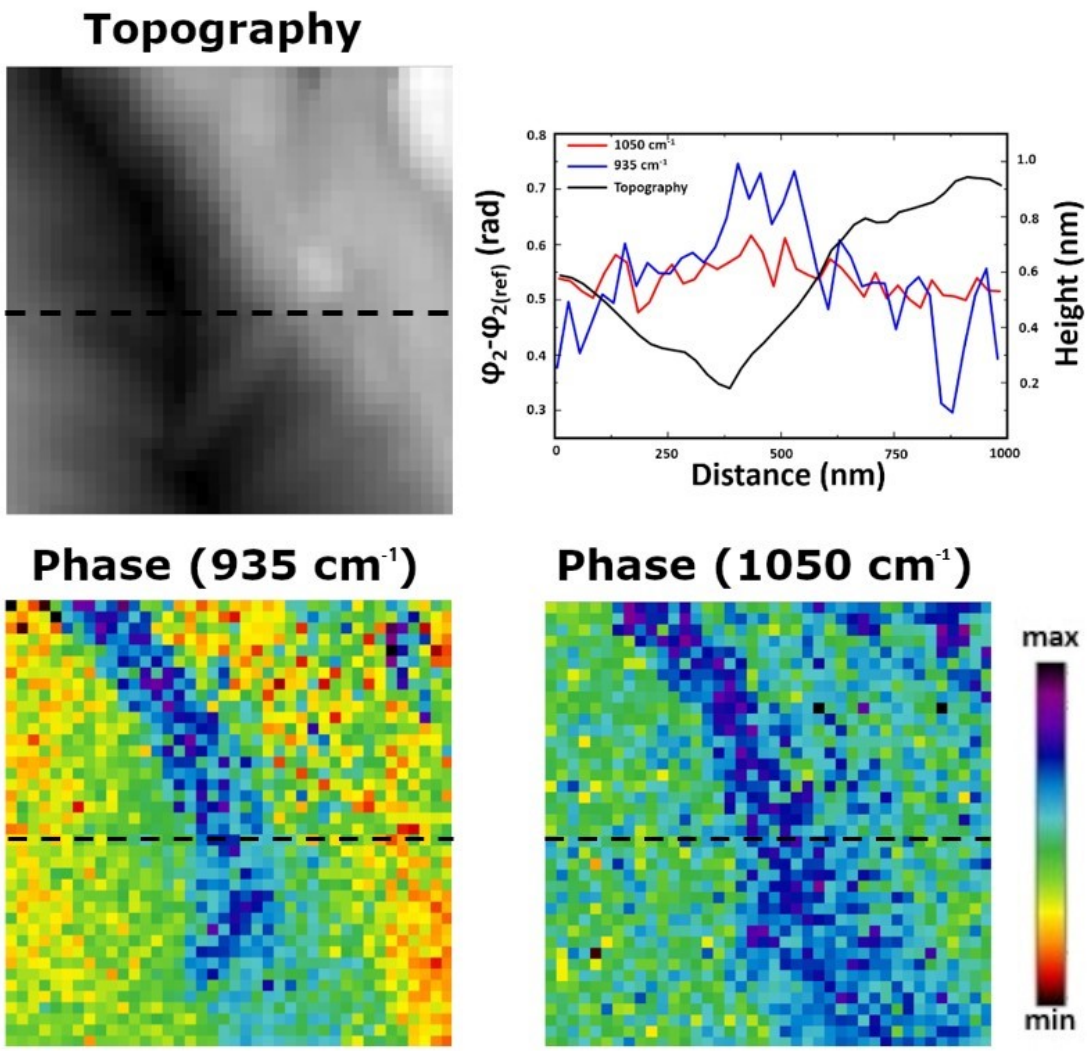

Figure S7. Topographical and phase images of lunar sample 15445.307 at both 935 cm^{-1} and 1050 cm^{-1} (similar to the amplitude images given in Figure 4c and 4d of the main text). The top right figure compares the topography and two phase images (similar to the amplitude in Figure 4b) for the dashed line shown in the topography image indicating that there is no correlation in the phase with height profile.

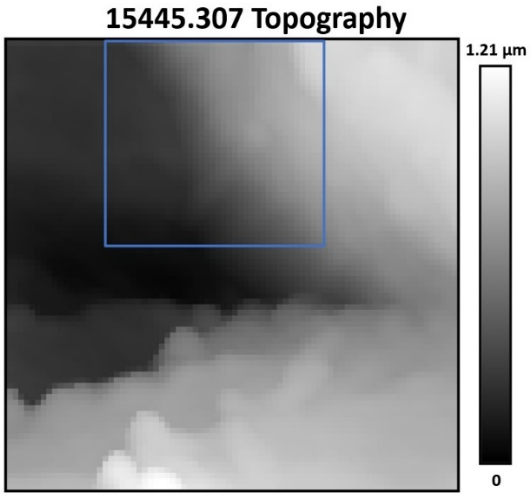

Figure S8. Topographical image of lunar sample 15445.307 for a 2,000 x 2,000 nm region. The truncated section indicated by the blue box was used for the line ratio analysis in Figure 4 in the manuscript and Figure S7.

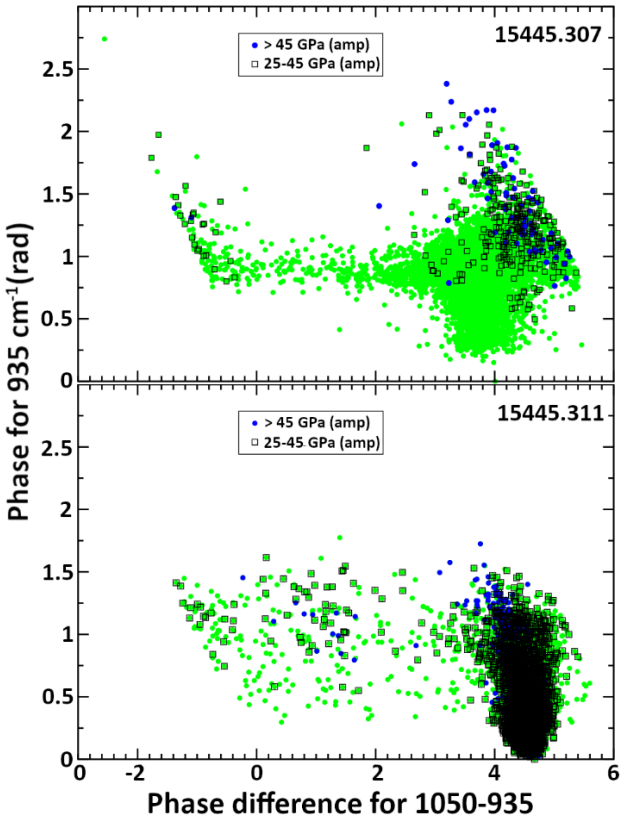

Figure S9. The nano-FTIR phase difference 1050 - 935 versus 935 cm^{-1} for 15445.307 (top) and 15445.311 (bottom) binned according to the reflectance ratios for shocked-induced pressure proposed in Ref. [1] as shown in Figure 4 of the manuscript.

3. Simulation Approach

In the extended dipole model, the scattered field is described by the complex-valued scattering coefficient and is derived from the near field interaction between the focused tip and sample surface [2,3]. The near field probe is represented by a spheroid made of metal inside a uniform electric field and is then reduced to a finite dipole consisting of two charges, one close to the sample and one further away. Only the closer charge has an impact on the near field interaction, causing an additional point charge to be induced close to the focus of the spheroid and its negative counterpart to be distributed along the focus. The two induced charges form a finite dipole from which is then used to describe the scattering between the focus and the sample surface.

The extended dipole model was used to simulate amorphous SiO_2 as discussed in the main text. As an example, the method is applied to simulate crystalline enstatite (E||a), as shown in Figure S10 for the Nano-FTIR amplitude and phase using the dielectric constants of Zeidler et al. [4]. These are compared to the reflectance spectra, typically relevant to flyby/orbital/remote observations, and the mass absorption coefficient. While the similarities in all three types of spectra are clear, there are minor shifts in peak energies and more pronounced shifts in peak heights. In contrast to weak oscillators (like biological samples or soft matter), the near-field spectra of strong Lorentz oscillators such as crystalline or amorphous minerals exhibit distinctive deviation from far-field spectra as evident in the blue-shifted peaks of the near-field as well as when compared to the real and imaginary parts of the dielectric constants. Further, at least in this case, the reflectance peaks appear much broader than the peaks in the real part of the dielectric constant and the Nano-FTIR amplitude.

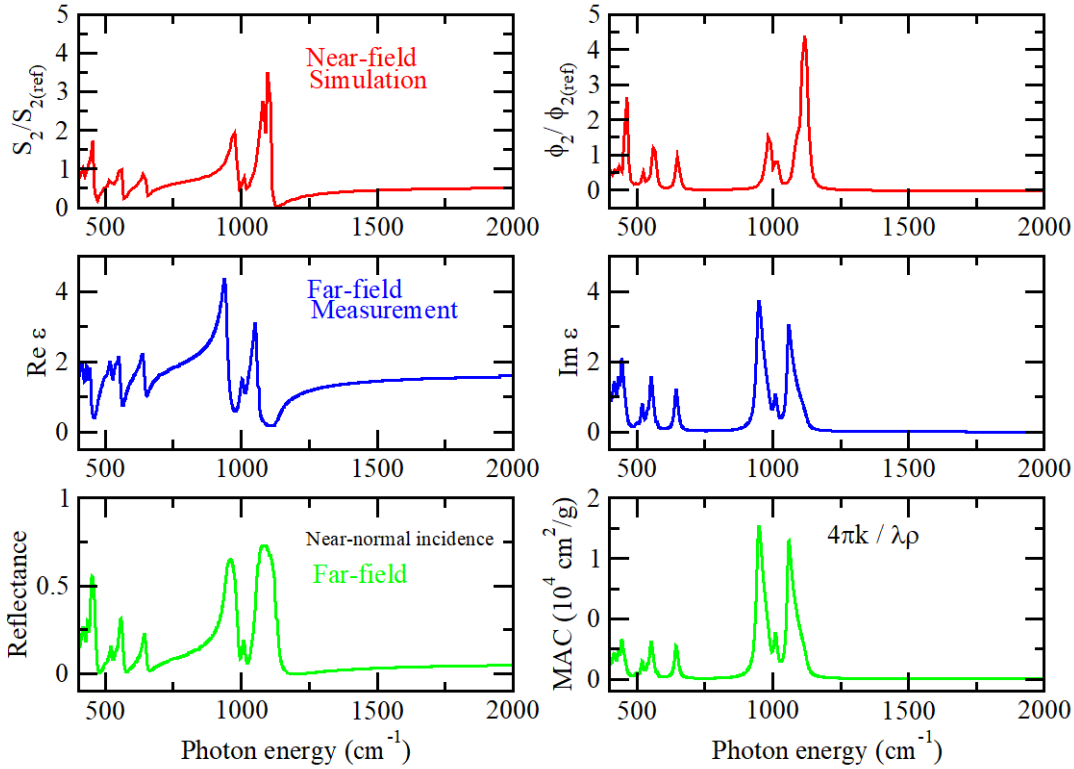

Figure S10. Optical properties of enstatite (E||a). Top row: simulated Nano-FTIR amplitude and phase (in rad). Middle row: real and imaginary parts for the enstatite (E||a) dielectric constants obtained from the far-field measurements of Zeidler et al. [4]. Bottom row: computed near-normal incident reflectance and mass absorption coefficient (MAC).

4. References

[1] Martin, D. J. P., et al. *Investigating the shock histories of lunar meteorites Miller Range 090034, 090070, and 090075 using petrography, geochemistry, and micro-FTIR spectroscopy*. Meteorit. Planet. Sci., 2017. **52**, 1103.

[2] Govyadinov, A.A., et al., *Quantitative Measurement of Local Infrared Absorption and Dielectric Function with Tip-Enhanced Near-Field Microscopy.* Journal of Physical Chemistry Letters, 2013. **4**(9): p. 1526-1531.

[3] Fali, A., et al., *Nanoscale Spectroscopy of Dielectric Properties of Mica.* ACS Photonics, 2021. **8**(1): p. 175-181.

[4] Zeidler, S., Mutschke, H., Posch, Th. *Temperature-Dependent Infrared Optical Constants of Olivine and Enstatite*, Astrophysical Journal 2015, **798**, 125.